Yrast γ-ray spectroscopy of the neutron rich isotopes ^{61,63}Co

P. H. Regan,[1,2] J. W. Arrison,[1,*] U. J. Hüttmeier,[1,†] and D. P. Balamuth[1]
[1]*Department of Physics and Astronomy, University of Pennsylvania, 209 South 33rd Street, Philadelphia, Pennsylvania 19104*
[2]*Department of Physics, University of Surrey, Guildford, GU2 5XH, United Kingdom*
(Received 29 April 1996)

The neutron rich nuclei ^{61,63}Co have been studied using the reactions ^{16}O(^{48}Ca,$p2n$)^{61}Co and ^{18}O(^{48}Ca,$p2n$)^{63}Co at a bombarding energy of 110 MeV. Discrete γ rays from the channels of interest were investigated using prescaled γ singles, charged-particle$-\gamma$, neutron$-$charged-particle$-\gamma$, and charged-particle$-\gamma-\gamma$ coincidence techniques. Decay schemes, with level spins deduced from two-point angular distribution data, are presented together with some approximate information on apparent state lifetimes. The experimental results are compared with previous light ion data for these systems and with theoretical shell model predictions. These data represent the first study of medium to high spin states in these nuclei. [S0556-2813(96)03909-X]

PACS number(s): 21.10.Hw, 23.20.En, 23.20.Lv, 27.50.+e

I. INTRODUCTION

The development of heavy ion accelerators has permitted extensive spectroscopic studies of high spin nuclear states through the use of fusion-evaporation reactions. However, because of the restriction to stable targets and projectiles, most of this work has focused on nuclei on the neutron deficient side of the valley of stability. While the data gained in such pursuits has provided a rich testing ground for present day nuclear models, the neutron rich side of the nuclear mass table remains much less explored.[1] For relatively light nuclei, however, it is possible to reach somewhat neutron rich systems by choosing high T_z beam/target combinations and studying the relatively low cross-section charged-particle evaporation channels [5,6]. Here we report results from a series of experiments using ^{48}Ca beams on a variety of light targets. This work can be thought of as an extension of the series of experiments carried out by Warburton and collaborators at Brookhaven National Laboratory in the 1970s [7–9] in which fusion-evaporation reactions were studied by bombarding a ^{48}Ca target with beams of various p-shell nuclei. In that work, attention was for the most part focused on the prolific xn evaporation channels. Here, we report on an investigation of ^{61,63}Co via the $p2n$ evaporation channel on ^{16,18}O targets. These nuclei have been studied previously via β decay [10,11] and light ion pickup and stripping experiments [12–16]. However, none of these experiments were able to identify the medium to high spin yrast states that are strongly favored by heavy ion fusion evaporation reactions.

The Co isotopes of interest have four or six neutrons outside of the $N = 28$ closed shell and may be understood within the framework of the spherical shell model. In particular, the location and density of yrast and near-yrast levels provide an excellent test of shell model calculations with different model spaces and residual interactions.

II. EXPERIMENTAL PROCEDURE

In order to identify γ-ray transitions in ^{61,63}Co, two separate experiments were performed at the University of Pennsylvania tandem Van de Graaff accelerator using gold backed $W^{16}O_3$ and $W^{18}O_3$ targets of thickness 400 μg/cm^2 and 1 mg/cm^2, respectively. The targets were bombarded by 110 MeV ^{48}Ca beams to populate states in the cobalt nuclei of interest via the $p2n$ evaporation channel. In-beam γ rays were identified using an array of six germanium detectors (three of which were Compton suppressed) operated in coincidence with the Penn 4π-segmented charged-particle detector array [17]. Three Ge detectors were placed at 90° with respect to the beam direction, two at 135° and one at 140°. The charged-particle phoswich array utilized the different time responses of the thin plastic (ΔE) and CaF_2 (stopping) scintillation detectors to distinguish between protons and α particles. A large unshielded tank of liquid scintillator was placed at 0° with respect to the incident beam to measure coincident neutrons. These were distinguished from the large γ-ray flux using time-of-flight information with respect to the charged-particle array. Data were written event by event to a write-once-read-many (WORM) optical disk on charged-particle$-\gamma$, neutron$-$charged-particle$-\gamma$, and charged-particle$-\gamma-\gamma$ coincidence events for off-line analysis. A prescaled sample of the γ-singles spectra was also measured simultaneously with the coincidence data.

Figures 1 and 2 show typical particle-γ coincidence spectra for the two reactions and illustrate the use of these spectra for identification of γ-ray transitions in the residual nucleus. Note how cleanly the charged-particle array resolves the different charged-particle channels. A proportion of the ^{16}O data has been subtracted from the ^{18}O data to account for the degree of contamination (approximately 20%) of ^{16}O in the isotopically enriched $W^{18}O_3$ target. (The degree of ^{16}O was deduced by comparing the yield to known strong xn channels

*Present address: Department of Physics, Villanova University, Villanova, Pennsylvania 19085.
†Present address: Seeliger and Partner, Otto-Beck-Strasse 32-34, D-68165 Mannheim, Germany.

[1]There have been a number of recent studies of yrast states in neutron rich fission fragments; the recent works by Aryaeinejad *et al.* [1], Durell [2], and Hotchkis *et al.* [3,4], and references therein, provide good examples of such work.

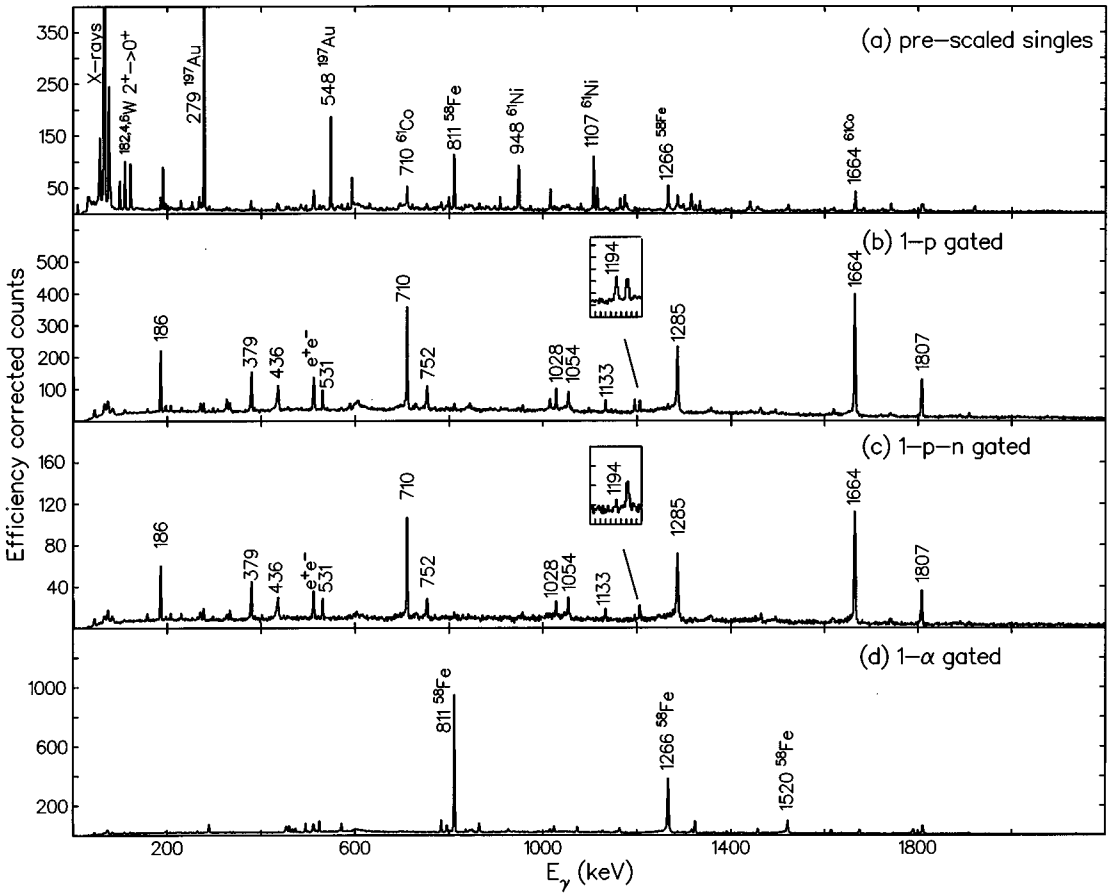

FIG. 1. Efficiency corrected spectra used to identify states in ^{61}Co. (a) The prescaled γ-singles data, (b) proton–γ (c) proton–neutron-γ, and (d) α-γ coincidence spectra from the ^{16}O+^{48}Ca reaction. Note the relative reduction in counts for the 1194 keV line from the pn channel to ^{62}Co compared to the more prominent $p2n$ lines from ^{61}Co.

in the prescaled γ-singles spectra in both targets [18].)

Some limited information is available on low lying levels of ^{61}Co and ^{63}Co from light ion studies [12,16]. It was nevertheless felt to be desirable to demonstrate experimentally that the observed transitions could be associated with a specific isotope. The following procedure was used. First, candidate transitions in cobalt isotopes were selected by requiring that they be present in the proton-γ coincidence spectra and absent in the α-γ coincidence spectra. (In these neutron rich systems, the probability of multiple charged-particle evaporation is sufficiently small to be neglected.) There then remains the problem of establishing the mass of the final nucleus. This was done by measuring the neutron multiplicity relative to neighboring cobalt isotopes in which transitions are known from previous work. Thus, states populated via $p2n$ evaporation were expected to have about two-thirds of the single neutron detection efficiency of the $p3n$ channel since only two-thirds as many neutrons are produced per event.

The procedure used is illustrated in Fig. 3(a) which plots the ratio of number of counts observed in the one-proton–neutron ($pn\gamma$) and one-proton ($p\gamma$) gated γ-ray singles spectra compared to several transitions in various Co isotopes in the ^{16}O+^{48}Ca reaction. Known transitions in ^{60}Co ($p3n$ evaporation) and ^{62}Co (pn) show apparent average neutron detection efficiencies of 0.47 ± 0.04 and 0.15 ± 0.03, respectively. Also observed are a group of transitions which are clustered around an apparent efficiency of 0.30 ± 0.03. The latter group is associated with transitions in ^{61}Co from $p2n$ evaporation. Most of these transitions were previously unknown. The strong 1284.5 keV transition which was assigned to ^{61}Co by Coop *et al.* using the $(p,\alpha\gamma)$ reaction [12] has an apparent efficiency of 0.32 ± 0.03, consistent with the expected value.

As Fig. 3(b) shows, states in ^{63}Co were identified in essentially the same manner as those in ^{61}Co, but using the ^{18}O target. Note, however, that the value of apparent detection efficiency for the $p2n$ lines from ^{63}Co is 0.21 ± 0.02, considerably less than for the $p2n$ channel in the ^{16}O reaction. We attribute this to a Q value effect; for the ^{16}O+^{48}Ca system, the available energy for the $p2n$ channel to ^{61}Co is 18.0 MeV, whereas for the ^{18}O reaction to ^{63}Co, 23.4 MeV is available. A semiquantitative estimate of the effect of this kinematic difference was made by assuming that (i) the proton in the $p2n$ evaporation is emitted at the Coulomb barrier, (ii) the residual nucleus has approximately 5 MeV in excitation energy, and (iii) the evaporated neutrons share the remaining energy equally. Knowing the neutron energy in the frame of the moving compound nucleus (we neglect the recoil due to proton emission) it is straightforward to calculate the effective solid angle available for detecting the neutron at zero degrees. This very crude estimate yields a prediction of 0.6 for the ratio of neutron detection

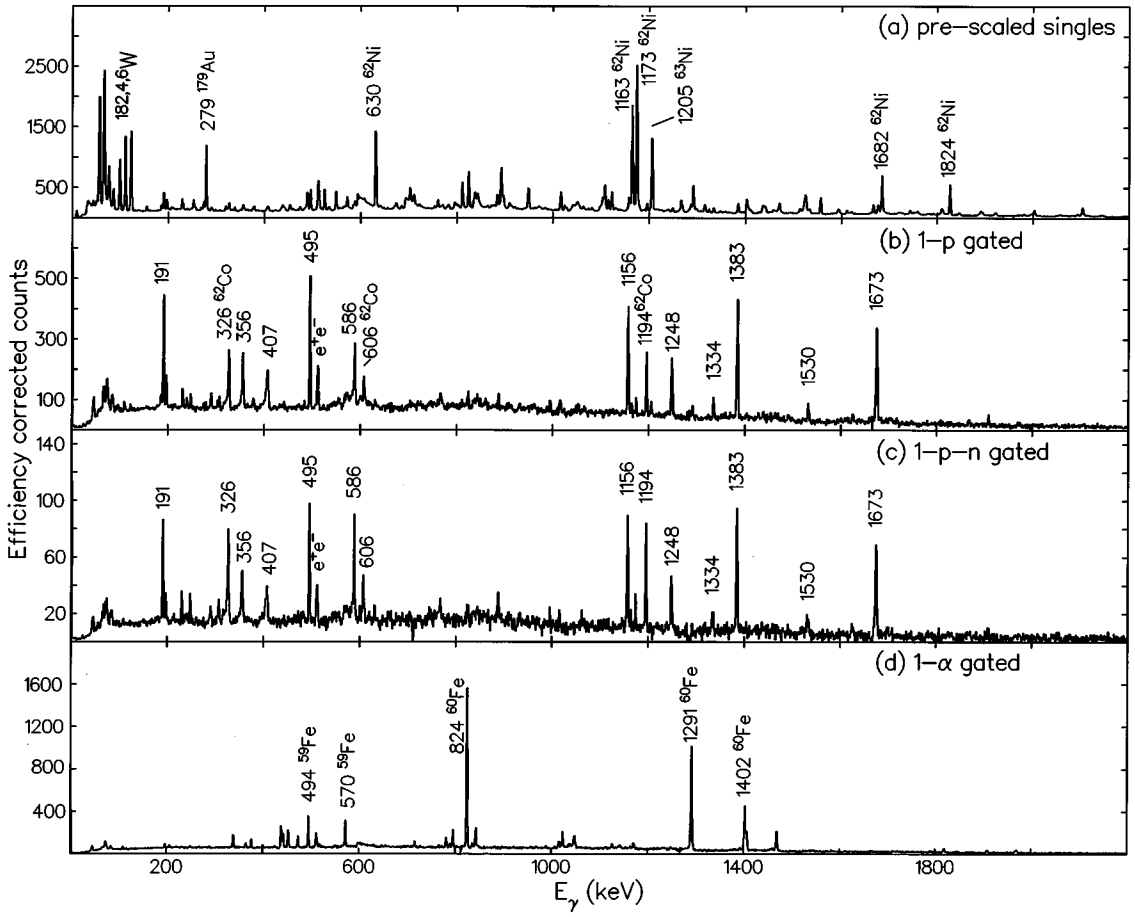

FIG. 2. Efficiency corrected spectra used to identify states in ^{63}Co. (a) The prescaled γ-singles data, (b) proton-γ (c) proton-neutron-γ, and (d) α-γ coincidence spectra from the ^{18}O+^{48}Ca reaction. Note a proportion of the corresponding ^{16}O data has been subtracted from each spectrum to account for the isotopic impurity of the target.

efficiency for the $p2n$ channel with the ^{16}O and ^{18}O beams. The observed ratio is 0.70 ± 0.10, in good agreement with this estimate.

The relative yields of the different final nuclei from the two reactions compared to the predictions of the fusion evaporation code CASCADE [19] are given in Tables I and II. The experimental values were taken from the prescaled γ-singles data, corrected for detector efficiency and relative γ-ray intensity. The strongest channel corresponds to xn evaporation in both cases; the preference for neutron emission is enhanced for the more neutron rich compound system. In the ^{18}O+^{48}Ca reaction, xn evaporation accounted for approximately 70% of the total cross section compared to 85% predicted by CASCADE. The data highlight the effectiveness of a high-efficiency charged-particle detector for studying such systems.

III. DECAY SCHEMES OF ^{61,63}Co

The decay schemes of ^{61,63}Co as deduced in the present work are shown in Figs. 4 and 5, respectively. These were constructed by investigating the coincidence relationships between transitions identified using the $p\gamma$ and $pn\gamma$ data. Strong lines were identified in the nuclei of interest using the apparent neutron detection efficiency technique described in Sec. II. A γ-γ matrix gated on the condition that a coincident proton was also observed in the 4π array was used to set coincidence gates on the candidate transitions. Typical examples of the p-γ-γ spectra used to build the decay schemes are shown in Figs. 6, 7, and 8.

Because the germanium detectors were restricted to essentially two angles (90° and $\approx$135°) with respect to the incident beam, only limited information was obtained on γ-ray angular distributions. If $P_k(\cos\theta)$ is the Legendre polynomial of order k and possible multipolarities are restricted to dipole and quadrupole, the angular distributions can be expressed as

$$W(\theta_\gamma)=A_0[1+a_2P_2(\cos\theta_\gamma)+a_4P_4(\cos\theta_\gamma)]. \quad (1)$$

In order to determine the intensity A_0 and the coefficients a_2 and a_4 from two data points, a simplifying assumption is necessary. We have made the usual one of setting a_4 to zero, which gives approximately correct values of A_0 and a_2 for both dipole and quadrupole transitions depopulating the highly aligned states populated in fusion evaporation reactions. The relative intensity A_0 and the observed coincidence relationships were used to deduce the ordering of the transitions in the decay schemes. The approximate values of a_2, obtained by measuring the anisotropy using the 90° and

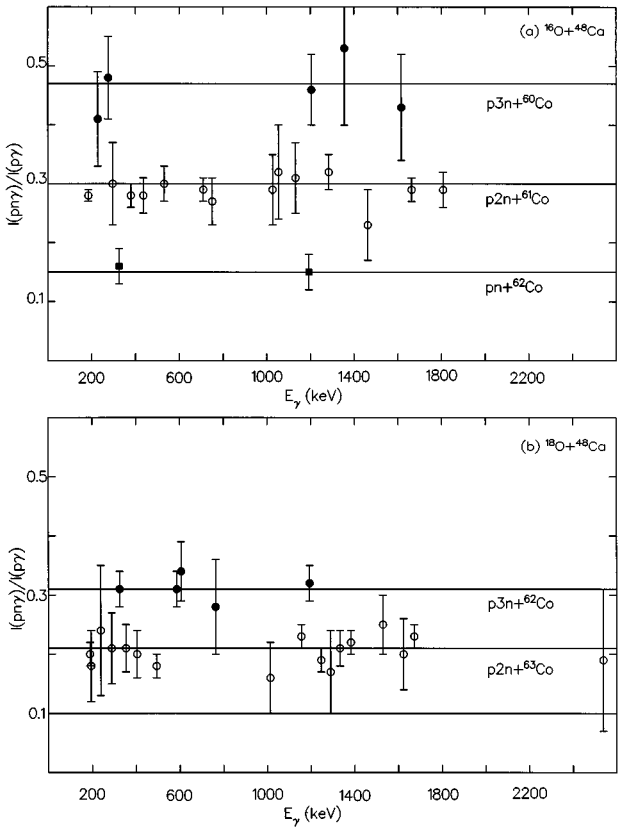

FIG. 3. Plot of ratio of relative intensities of states in proton-neutron-γ and proton-γ spectra, identified in (a) the ^{16}O+ ^{48}Ca and (b) the ^{18}O+ ^{48}Ca reactions. Note how the neutron multiplicities, used to identify the residual decay products, are clearly separated.

135° detectors,[2] were used to suggest multipolarities for the observed transitions as follows: (a) A negative value of a_2 is expected for a $J\rightarrow J-1$ dipole transition, (b) a positive a_2 is expected for a $J\rightarrow J-2$ quadrupole transition or a $J\rightarrow J$ dipole transition. Mixed dipole/quadrupole transitions can have either positive or negative values of a_2. In addition, it was assumed that most of the electromagnetic cascades following fusion evaporation reactions populate yrast or near-yrast states whose spins decrease as the nucleus cools towards the ground state.

While the parity of the transitions could not be assigned experimentally, since neither γ-ray polarization nor internal conversion was measured, it is most likely that the lower lying yrast levels have negative parity due to the filling of f and p neutron orbitals near the Fermi surface coupled to a $\frac{7}{2}^-$ proton hole. However, at sufficiently high excitation energy, positive parity states will approach the yrast line due to the population of the positive parity $g_{9/2}$ neutron orbital. For example, in the neighboring $N = 34$ and 36 isotones ^{62}Ni [9,20] and ^{64}Ni [21] the lowest non-normal-parity states occur at an excitation energy of approximately 3.5 MeV. This suggests that positive parity must be considered for states in ^{61,63}Co with $J>13/2$. For spectroscopic purposes, we have in general refrained from making definite parity assignments to states with $E_x> 2$ MeV. For some levels limited information concerning level parities can be inferred from the level scheme and limits on lifetimes obtained from measurements of experimental Doppler shifts. These are discussed below.

[2]Care was taken to include any Doppler shifted components of line shapes in the 135° detectors when determining this anistropy.

TABLE I. Comparison of experimental and predicted relative cross sections for the reaction ^{16}O+ ^{48}Ca at 110 MeV. The yields are quoted as percentages of the total yield.

Nucleus	Channel	σ_{expt} (%)	σ_{cas} (%)
^{62}Ni	$2n$	9(2)	1
^{62}Co	pn	1(1)	0.2
^{61}Ni	$3n$	30(5)	48
^{61}Co	$p2n$	22(3)	14
^{60}Ni	$4n$	6(1)	22
^{60}Co	$p3n$	1(1)	4
^{58}Fe	$\alpha 2n$	27(4)	11

A. ^{61}Co

The decay scheme constructed for ^{61}Co in the present work is shown in Fig. 4 and summarized in Table III. A ground-state spin of $\frac{7}{2}^-$ has been deduced for ^{61}Co following the β decay of ^{61}Fe [10]. The low lying $\frac{9}{2}^-$ and $\frac{11}{2}^-$ states at excitation energies of 1285 keV and 1664 keV have been identified previously by Mateja *et al.* [13] using the ^{64}Ni (p,α) ^{61}Co reaction. The 1285 keV transition was identified by Coop *et al.* [12] using $(p,\alpha\gamma)$ coincidence measurements. The observation of the 298 and 1028 keV lines in the present data appears to confirm the work of Coop *et al.* who identified these decays from the non-yrast 1326 and 1028 keV states, respectively. The a_2 values for both the 298 and 1028 keV lines suggest an isotropic angular distribution, consistent with the previous $\frac{1}{2}^-$ assignment for the 1326 keV state. None of the other non-yrast states observed in these previous works were seen in the present study. Conversely, the high spin yrast levels observed in the present work constitute previously unidentified states, consistent with the expectation that heavy ion fusion reactions preferentially populate near-yrast states.

Figure 6(c) shows the gate on the 709/710 keV doublet in ^{61}Co. The placement of these two transitions in the decay scheme was facilitated by information from the coincidence spectra. The intensity of the 709 keV transition depopulating the level at E_x=4802 keV, was deduced by adding the 1807 and 186 keV gates and comparing the observed intensity of the 709 keV line in this spectrum with that of the 436 keV

TABLE II. Comparison of experimental and predicted relative cross sections for the reaction ^{18}O+ ^{48}Ca at 110 MeV. The yields are quoted as percentages of the total cross sections.

Nucleus	Channel	σ_{expt} (%)	σ_{cas} (%)
^{63}Ni	$3n$	30(5)	12
^{63}Co	$p2n$	7(1)	2
^{62}Ni	$4n$	38(6)	73
^{62}Co	$p3n$	6(1)	6
^{60}Fe	$\alpha 2n$	12(2)	3
^{59}Fe	$\alpha 3n$	7(1)	3

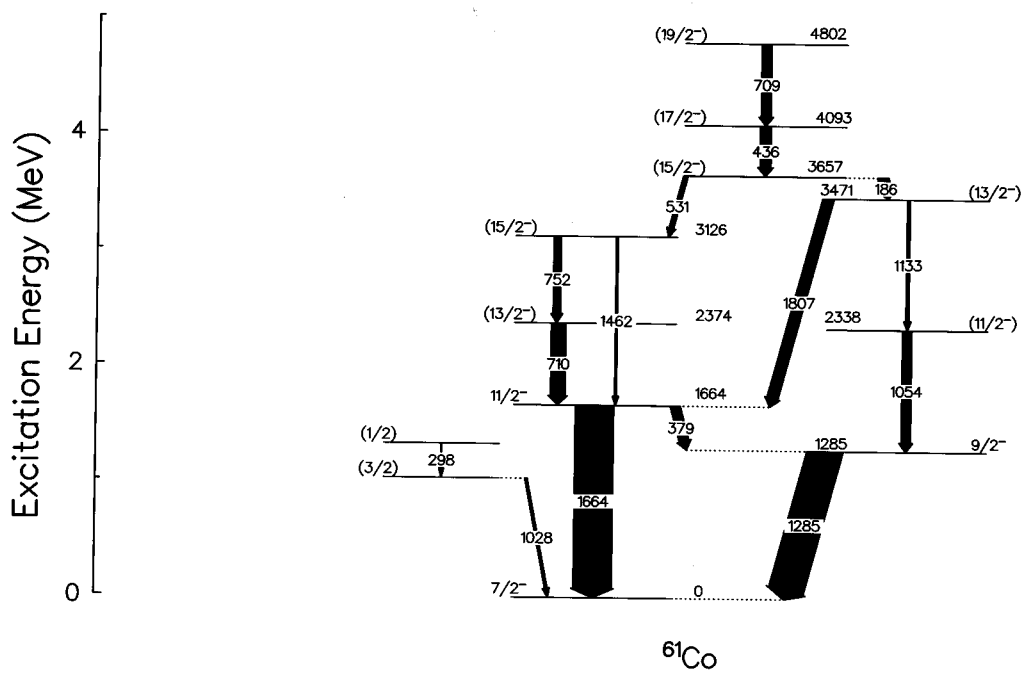

FIG. 4. Partial decay scheme for ^{61}Co as deduced in the present work.

transition. The intensity of the 710 keV γ ray depopulating the 2374 keV state was then calculated by subtracting the normalized intensity of the 709 keV transition depopulating the 4802 keV state from the value measured for the doublet in the one-proton gated spectra.

The $\Delta I=1$ assignment for both members of the 752–710 keV cascade linking the 3126 and 1664 keV states is strengthened by the observation of the 1462 keV crossover transition. The measured value for the 1462 keV line of $a_2=+0.50\pm0.51$ is consistent with a $\Delta I=2$, pure electric quadrupole transition and a $I=15/2$ assignment to the 3126 keV state. The a_2 value deduced for the 709/710 keV doublet in the p-γ singles data is -0.16 ± 0.12, implying a $\Delta I=1$ transition. As the observed a_2 value for the doublet is comparable to the values of the 752 keV transition which is assigned as $\Delta I=1$ ($a_2=-0.24\pm0.21$), both γ rays in the 709/710 keV doublet are assigned as $\Delta I=1$.

The measured a_2 values for the 1054, 1133, and 1807 keV lines of -0.27 ± 0.19, $+0.06\pm0.29$, and -0.13 ± 0.14, respectively, are all consistent with $\Delta I=1$; note that the 1133 keV transition shows some evidence of a nonzero quadrupole admixture. Taken together, this information strongly favors an $I=13/2$ assignment for the 3471 keV state, with negative parity favored since $M2/E1$ mixtures are not expected to occur. Similarly, assuming a mixed $E2/M1$, $\Delta I=1$ transition for the 186 keV line ($a_2=-0.10\pm0.13$) decaying from the 3657 keV level to the state at 3471 keV implies an $I=15/2$ assignment for the 3657 keV state, with negative parity also favored. This assignment requires the 531 keV γ ray, which links the 3657 and 3126 keV states, to

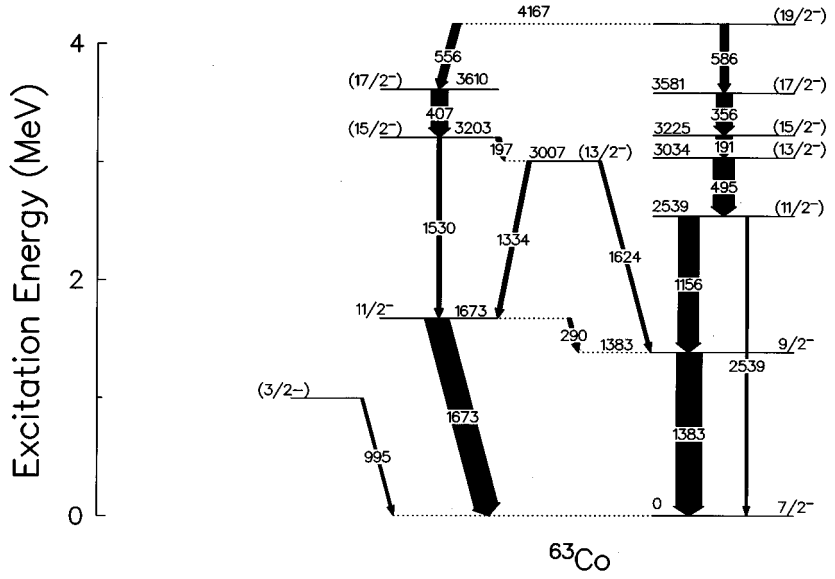

FIG. 5. Partial decay scheme for ^{63}Co as deduced in the present work.

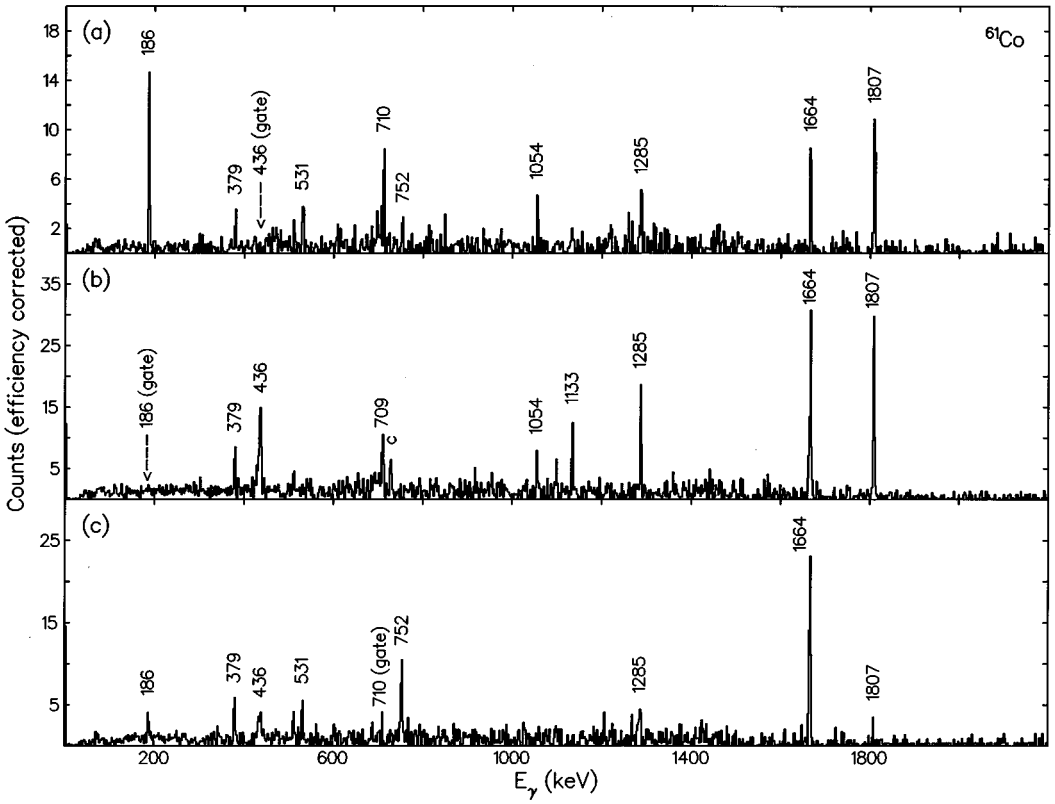

FIG. 6. Examples of efficiency corrected one-proton–γ–γ coincidence spectra used to build up the decay scheme for ^{61}Co.

be an unstretched dipole, $\Delta I=0$ transition. The measured a_2 value of $+0.45\pm0.29$ for the 531 keV line is consistent with this interpretation.

As in previous studies of nuclei in this region (e.g., Ref. [9]), the data revealed a considerable amount of fast side feeding, even at low excitation energy. A good example of this effect is given by the 1285 keV $\frac{9}{2}^- \rightarrow \frac{7}{2}^-$ transition. The sum of the γ-ray intensities of the 379 and 1054 keV transitions which feed this state sums to 55 ± 7, while the measured intensity of the 1285 keV line is 102 ± 9, implying that almost 50% of the intensity which feeds this state comes from continuum decays not discretely distinguished in the present work. As Fig. 9 shows, this side feeding gives rise to a large Doppler shifted component in the γ-ray line shape of this transition. If the observed discrete feeding for the 1285 keV line is sufficiently slow for the nucleus to be stopped by the time the 1285 keV state decays (a sensible assumption since both the 379 and 1054 keV lines show rather smaller Doppler shifts than the 1285 keV line), it is reasonable to assume that most of the shifted component of the 1285 keV line shape is due to feeding from short-lived continuum states. An estimate of the relative intensity of the fast side feeding compared to the slower discrete feeding can be obtained by comparing the intensity of the stopped and shifted components of the line shape of the 1285 keV line at 135°. We deduce that the shifted component of the line shape makes up 0.46 ± 0.15 of the total 1285 keV intensity. This compares extremely well with the side feeding intensity as deduced by comparing the discrete intensities above and below the 1285 keV state.

B. ^{63}Co

The decay scheme constructed for ^{63}Co in the present work is shown in Fig. 5 and summarized in Table IV. The $\frac{7}{2}^-$ ground state of ^{63}Co has been deduced from β^- decay studies of ^{63}Fe [11]. The low lying $\frac{9}{2}^-$ and $\frac{11}{2}^-$ states at $E_x=$ 1383 and 1673 keV, respectively, have been previously observed by Seeger *et al.* using the $(d,{}^3\mathrm{He})$ reaction [16]. However, the spin proposed in the present work for the 1383 keV state differs from the previous assignment. Seeger *et al.* assigned a spin of (5/2,7/2) to the 1383 level on the basis of an $l=3$ assignment for the angular distribution, leading to this level in the $(d,{}^3\mathrm{He})$ reaction. In the present work, the observation of a $\Delta I=1$ decay to the $\frac{7}{2}^-$ ground state (1383 keV transition) and the observation of γ rays connecting this state to the previously observed $\frac{11}{2}^-$ state at excitation energy 1673 keV strongly suggests $I^\pi=\frac{9}{2}^-$ for the 1383 keV level. The $I^\pi=\frac{11}{2}^-$ assignment for the 1673 keV level is consistent with the $l=5$ assignment of Seeger *et al.* [16]. Possible explanations for the ambiguity in the spin assignment of the 1383 keV state between the work of Seeger *et al.* and the present study include the presence of two levels with similar energies and, more likely, the difficulty in assigning l values to states weakly populated in pickup and stripping reactions.

The observation of the 2539 keV transition across the 1156–1383 keV $\Delta I=1$ transitions strongly suggests a $I=11/2$ assignment for the 2539 keV state, with negative parity favored. The members of the 495-191-356 cascade all have a_2 values which imply $\Delta I=1$ transitions. The ordering of these states is based primarily on intensity information,

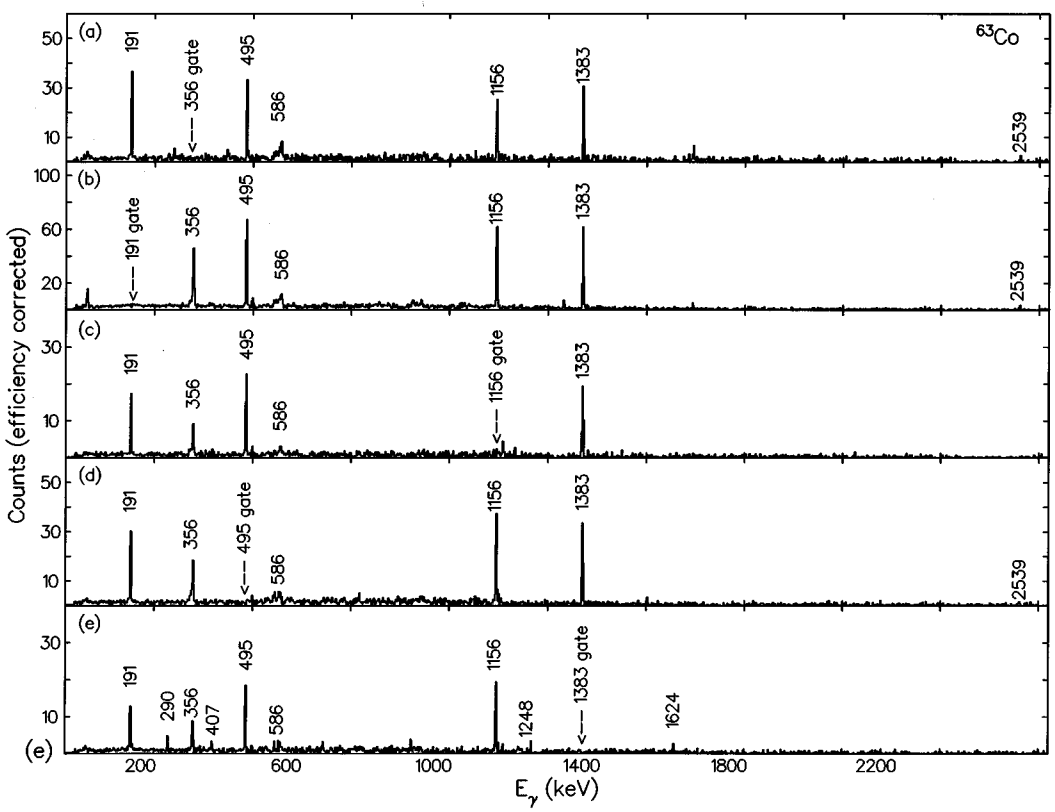

FIG. 7. Efficiency corrected one-proton$-\gamma-\gamma$ coincidence spectra used to build up the right-hand side of the decay scheme for ^{63}Co shown in Fig. 5.

although it should be noted that the 356 and 191 keV transitions have equal intensities within experimental errors. However, since the 356 keV line has an appreciable Doppler shifted component in its line shape, it was placed above the 191 keV line which was almost completely stopped. Unfortunately, as a result of a strong contaminant in ^{62}Co, an accurate measurement for the angular distribution of the 586 keV transition was not possible in the present work.

A tentative spin of (19/2) could, however, be assigned to the 4167 keV state from the parallel decay path through the 556, 407, and 1530 keV transitions down to the yrast $\frac{11}{2}^-$ state at 1673 keV (see Fig. 8). We note that the excitation energy of the yrast 19/2 state is the same when deduced by adding up the energies of the individual transitions in the two decay paths to well within the experimental errors. This, together with the experimental observation that the 556 and 586 keV lines have equal fractional Doppler shifts (see next section), strongly suggests that both transitions originate from the same state. Note that the quadrupole assignment to

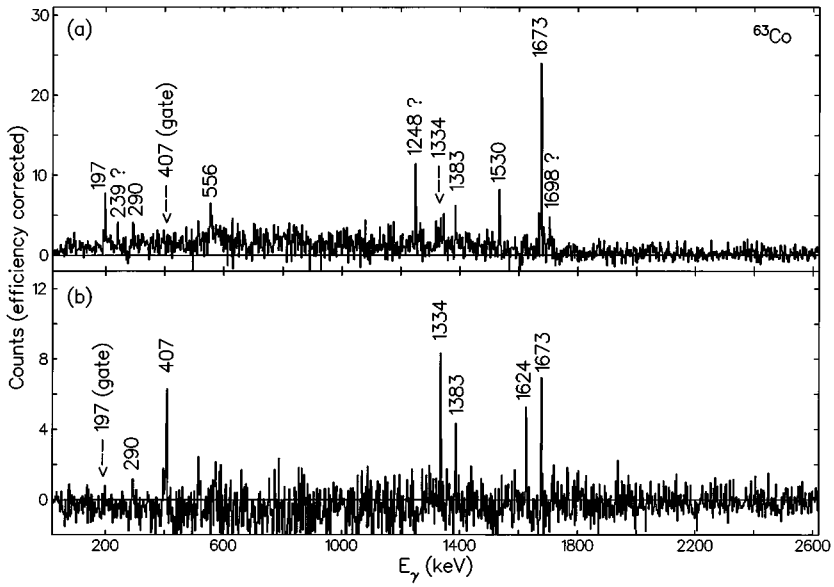

FIG. 8. Efficiency corrected one-proton gated γ-γ coincidence gates on the 197 and 407 keV lines in ^{63}Co. Note the 239, 1248, and 1698 keV transitions in the 407 keV gate.

TABLE III. Transitions identified in ^{61}Co. Unless otherwise stated the intensities are taken from the p-γ data.

E_γ (keV)	$\frac{I(pn)}{I(p)}$	$E_i \rightarrow E_f$ (keV)	Intensity	$\frac{W(135)}{W(90)}$	a_2	$J_i^\pi \rightarrow J_f^\pi$ [a]
186.4(5)	0.28(1)	3657→3471	32(4)	0.93(9)	−0.10(13)	$(\frac{15}{2}^- \rightarrow \frac{13}{2}^-)$
298.0(7)[b]	0.30(7)	1326→1028[b]	1(1)	1.14(43)	+0.17(38)	$(\frac{1}{2}^- \rightarrow \frac{3}{2}^-)$
379.1(5)	0.28(2)	1664→1285	28(4)	0.97(12)	−0.04(15)	$\frac{11}{2}^- \rightarrow \frac{9}{2}^-$
435.7(5)	0.28(3)	4093→3657	31(5)	0.91(11)	−0.13(15)	$(\frac{17}{2}^- \rightarrow \frac{15}{2}^-)$
531.2(5)	0.30(3)	3657→3126	13(3)	1.43(30)	+0.45(29)	$(\frac{15}{2}^- \rightarrow \frac{15}{2}^-)$
708.5(1.5)	0.29(2)[c]	4802→4093	31(6)	0.89(8)[c]	− 0.16(12)[c]	$(\frac{19}{2}^- \rightarrow \frac{17}{2})$
710.0(5)		2374→1664	47(6)[d]	–	–	$(\frac{13}{2}^- \rightarrow \frac{11}{2}^-)$
752.4(5)	0.27(4)	3126→2374	20(4)	0.84(14)	−0.24(21)	$(\frac{15}{2}^- \rightarrow \frac{13}{2}^-)$
1028.0(5)[b]	0.29(6)	1028→0[b]	7(1)	0.91(20)	−0.13(27)	$(\frac{3}{2}^- \rightarrow \frac{7}{2}^-)$
1053.9(7)	0.32(8)	2338→1285	27(6)	0.82(14)	−0.27(19)	$(\frac{11}{2}^-) \rightarrow \frac{9}{2}^-$
1133.3(7)	0.31(6)	3471→2338	8(3)	1.05(27)	+0.06(29)	$(\frac{13}{2}^- \rightarrow \frac{11}{2}^-)$
1284.5(6)	0.32(3)	1285→0	102(9)	1.17(8)	+0.20(8)	$\frac{9}{2}^- \rightarrow \frac{7}{2}^-$
1462.4(8)	0.23(6)	3126→1664	5(2)	1.52(50)	+0.50(50)	$(\frac{15}{2}^-) \rightarrow \frac{11}{2}^-$
1663.8(7)	0.29(2)	1664→0	110(16)	1.35(17)	+0.38(13)	$\frac{11}{2}^- \rightarrow \frac{7}{2}^-$
1806.5(1.0)	0.29(3)	3471→1664	32(4)	0.91(10)	−0.13(14)	$(\frac{13}{2}^-) \rightarrow \frac{11}{2}^-$

[a]See text for discussion on specific spin/parity assignments.
[b]Previously observed in non-yrast studies [12].
[c]Value for the unresolved doublet; see discussion in text.
[d]Deduced from p-γ-γ data.

the 1530 keV γ ray strongly suggests negative parity for the $E_x = 3203$ keV state.

A number of relatively intense transitions (239, 1248, and 1698 keV) were identified as coming from the decay of ^{63}Co but could not be definitively placed in the decay scheme in the present work. The 1248 keV γ ray was observed particularly strongly in the 407 keV gate (see Fig. 8). However, after an exhaustive search, no evidence of a linking transition or transitions between the 407 keV and the 1248 keV γ rays could be found.

IV. LIFETIME MEASUREMENTS AND LEVEL PARITIES

The lifetimes of nuclear states of the order of picoseconds can be measured using the Doppler shift attenuation method [22]. If a transition of energy E_0 from a recoiling nucleus traveling with velocity $v(t)$ at time t is detected at an angle θ with respect to the recoil direction, the measured energy will be Doppler shifted to a value E_s. To first order in v/c,

$$E_s = E_0\left(1 + \frac{v(t)}{c}\cos\theta\right), \tag{2}$$

where c is the speed of light in vaccuo. If v_0 is the initial velocity of the recoil as it is created and $v_{\rm av}$ is the average recoil velocity when the γ ray is emitted, the fractional Doppler shift $F(\tau)$ is given by

$$F(\tau) = \frac{1}{v_0}\int_0^\infty v(t)e^{-\frac{t}{\tau}}dt = \frac{v_{\rm av}}{v_0}. \tag{3}$$

The cleanliness of the particle-γ coincidence spectra available using the Penn 4π array allowed the recoil-γ data to be used to measure a number of experimental fractional Doppler shifts. The three detectors at 90° to the beam direction (where the first order Doppler shift is zero) were used to determine the transition energies, while the average shifted energies were obtained by measuring the centroids of the backward shifted peaks in the two 135° detectors. Corrections for second order Doppler shift, while in principle important for a fully shifted high energy gamma ray, were negligible for the transitions studied and were not included. Typical examples of the spectra used to obtain these data are shown in Figs. 9 and 10.

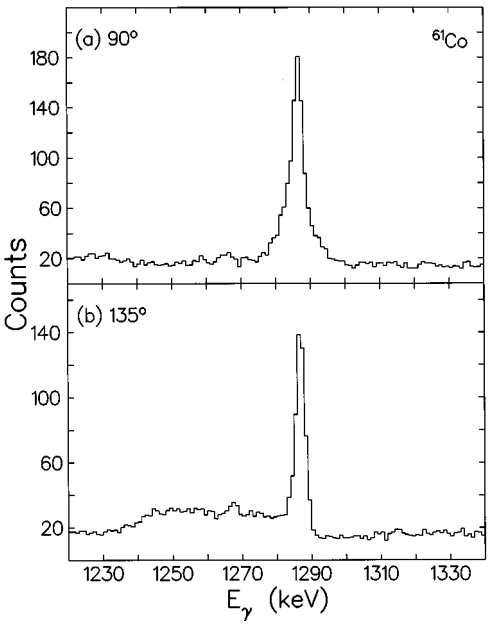

FIG. 9. Angle gated, one-proton−γ spectra showing the line shape of the 1285 keV $\frac{9}{2}^- \rightarrow \frac{7}{2}^-$ line in ^{61}Co.

In the case of the 586 keV transition in ^{63}Co an accurate value for the shifted centroid could not be obtained from the p-γ singles data due to the presence of a strong contaminant transition from ^{62}Co. In this case, an estimate for the shifted centroid was obtained from the proton gated γ-γ coincidence spectra. A two-dimensional (2D) coincidence matrix of $E_\gamma(90°)$ vs $E_\gamma(135°)$ was constructed. Gates were then set on the unshifted lines on the 90° axis and the associated coincidences were projected onto the 135° axis. Inspection of the 135° spectra allowed the fractional Doppler shift to be obtained. The projection of the sum of a number of transitions in coincidence with the 586 keV line in ^{63}Co is shown in Fig. 11.

The maximum initial velocities of the ^{61}Co and ^{63}Co recoils were calculated from the reaction kinematics to be 5.24% and 5.08% at the speed of light, respectively. These values do not take the change of mass due to the emission of light particles into account and are calculated using conservation of momentum of the target, beam, and compound nucleus before and after fusion. Assuming that the recoils were created halfway through the target on average, an average starting velocity of 5.1% and 5.0% of c was used.

In order to convert the experimentally derived $F(\tau)$ values to mean lifetimes, knowledge of the slowing down process of the recoil as it traversed through the target and backing material was required. The experimental $F(\tau)$ values were converted to apparent lifetimes assuming Lindhard-Scharff-Schiott (LSS) stopping theory [23]. The relatively large recoil velocity implies that the slowing down process is dominated by the electronic component; the influence of the less well understood nuclear stopping is quite small. Table V gives a summary of the Doppler shift attenuation method (DSAM) results for shifted transitions observed in the present work. Because of the incomplete nature of the decay schemes, the nature of feeding into these transitions is not well known. For this reason, the intrinsic lifetimes of the states could not be accurately deduced and therefore only the *apparent* lifetimes, which are at least as long as the actual lifetimes, are quoted.

These lifetimes can be used to obtain lower limits for the $B(M1)$, $B(E1)$, and $B(E2)$ strengths for the observed transitions since, in Weisskopf units [24],

$$B(M1)=\frac{3.2\times10^{-14}}{E_\gamma^3\,(\mathrm{MeV})\times\tau_{\mathrm{expt}}\,(\mathrm{sec})}, \tag{4}$$

$$B(E1)=\frac{1.0\times10^{-14}}{A^{2/3}\,E_\gamma^3\,(\mathrm{MeV})\times\tau_{\mathrm{expt}}\,(\mathrm{sec})}, \tag{5}$$

and

$$B(E2)=\frac{1.4\times10^{-8}}{A^{4/2}E_\gamma^5\,(\mathrm{MeV})\times\tau_{\mathrm{expt}}\,(\mathrm{sec})}. \tag{6}$$

Note that the lower limits for the $B(M1)$ strengths quoted in Table V assume no electric quadrupole admixtures.

The lifetime data obtained for the four $\Delta I=1$ transitions in ^{63}Co shown in Table V (the 356, 407, 556, and 586 keV γ rays) can be used to infer their magnetic rather than electric dipole nature. If any of these were an electric dipole

TABLE IV. Transitions identified in ^{63}Co. The quoted intensities are relative to 100% intensity to the ground state and measured from the p-γ unless otherwise stated.

E_γ (keV)	$I(pn)/I(p)$	$E_i\rightarrow E_f$ (keV)	Intensity	$\frac{W(135)}{W(90)}$	a_2	$J_i^\pi\rightarrow J_f^\pi$ [a]
191.3(4)	0.20(2)	3225→3034	45(5)	0.96(9)	−0.05(11)	$(\frac{15}{2}^-\rightarrow\frac{13}{2}^-)$
196.8(4)	0.18(6)	3203→3007	15(5)	0.89(23)	−0.16(29)	$(\frac{15}{2}^-\rightarrow\frac{13}{2}^-)$
239.1(4)[b]	0.24(11)	–	6(3)	–	–	–
290.3(4)	0.21(6)	1673→1383	10(4)	0.88(30)	−0.18(39)	$\frac{11}{2}^-\rightarrow\frac{9}{2}^-$
355.7(4)	0.21(4)	3581→3225	44(7)	0.85(10)	−0.22(15)	$(\frac{17}{2}^-\rightarrow\frac{15}{2}^-)$
407.0(5)	0.20(4)	3610→3203	47(8)	0.89(11)	−0.16(16)	$(\frac{17}{2}^-\rightarrow\frac{15}{2}^-)$
495.0(5)	0.18(2)	3034→2539	58(6)	0.91(7)	−0.13(10)	$(\frac{13}{2}^-\rightarrow\frac{11}{2}^-)$
555.9(8)	0.19(5)	4167→3610	22(7)	0.89(19)	−0.16(26)	$(\frac{19}{2}^-\rightarrow\frac{17}{2}^-)$
585.8(1.0)	0.31(3)[c]	4167→3581	30(4)[d]	–	–	$(\frac{19}{2}^-\rightarrow\frac{17}{2}^-)$
995.0(5)[e]	0.27(12)	995→0	6(1)	–	–	$\frac{3}{2}^-\rightarrow\frac{7}{2}^-$
1156.1(7)	0.23(2)	2539→1383	56(5)	0.89(7)	−0.16(11)	$(\frac{11}{2}^-\rightarrow\frac{9}{2}^-)$
1247.6(7)[b]	0.19(2)	–	32(8)	1.35(28)	+0.38(20)	–
1333.5(1.0)	0.21(3)	3007→1673	11(4)	1.13(29)	+0.16(40)	$(\frac{13}{2}^-)\rightarrow\frac{11}{2}^-$
1382.6(1.0)	0.22(2)	1383→0	72(6)	0.99(7)	−0.01(8)	$\frac{9}{2}^-\rightarrow\frac{7}{2}^-$
1530.4(1.0)	0.25(5)	3203→1673	12(4)	1.15(33)	+0.18(45)	$(\frac{15}{2}^-)\rightarrow\frac{11}{2}^-$
1623.9(1.0)	0.20(5)	3007→1383	9(4)	–	–	$(\frac{13}{2}^-)\rightarrow\frac{9}{2}^-$
1673.2(1.0)	0.23(2)	1673→0	66(8)	1.24(12)	+0.28(13)	$\frac{11}{2}^-\rightarrow\frac{7}{2}^-$
1698.4(1.5)[b]	–	–	10(4)[d]	–	–	–
2538.7(1.5)	0.19(12)	2539→0	5(2)	–	–	$(\frac{11}{2}^-\rightarrow\frac{7}{2}^-)$

[a]See text for discussion on specific spin/parity assignments.
[b]Not placed in decay scheme.
[c]Contaminant from ^{62}Co.
[d]Intensity deduced from p-γ-γ data.
[e]Observed previously in β decay studies.

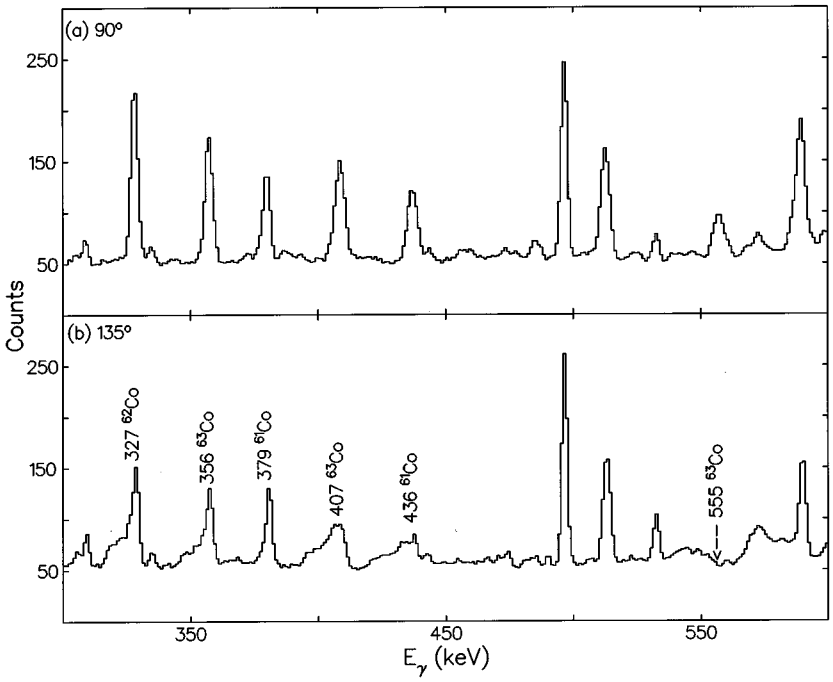

FIG. 10. Proton-γ coincidence data for detectors at (a) 90° and (b) 135° for the $^{18}O+^{48}Ca$ from which the fractional Doppler shift data on ^{63}Co was taken. Note the presence of strong shifted ^{61}Co lines from the ^{16}O target contaminant.

transition, the lower limit for the states lifetime would imply an extremely large $E1$ strength of approximately 10^{-2} Weisskopf units (W.u.). Typical values for $E1$ strengths in this region are two or three orders of magnitude smaller than this [25]. The recommended upper limit (RUL) for $E1$ transitions for $A = 45$–90 is 0.01 W.u. Of the 127 transitions studied in [25] only 2 have strengths larger than 10^{-3} W.u. The lower limits for the $M1$ strengths for these transitions are by contrast within the expected values for these nuclei [25], strongly suggesting magnetic dipole (or mixed $E2/M1$) assignments for these decays. A similar argument applies to the 436 keV transition in ^{61}Co. Given the arguments in the preceding paragraph we can infer that the parities of the $E_x = 3657$ and 4093 keV levels in ^{61}Co are the same. In ^{63}Co, if we accept negative parity for the 3203 keV level based on an assumed $E2$ assignment to the 1530 keV γ ray, the $M1$ nature of the 407 and 556 keV γ rays implies negative parity for the $E_x = 3610$ and 4167 keV levels. In turn, taking the 586 and 356 keV transitions as $M1$'s implies negative parity for the $E_x = 3581$ and 3223 keV levels. Because of the relatively weak evidence concerning the parities of excited states, we have not quoted definitive parity assignments for any levels observed in this work with $I > \frac{11}{2}$.

TABLE V. Measured fractional Doppler shifts and lifetimes for shifted states in $^{61,63}Co$.

Nucleus	E_0 (keV)	E_s (keV)	$\frac{v}{c}$ (%)	$F(\tau)$	τ_{app} (ps)	$B(M1)$[a] (W.u.)	$B(E1)$[b] (W.u.)
^{61}Co	379.1(5)	378.5(4)	0.2(1)	0.04(2)	10^{+10}_{-3}	$0.012^{+0.010}_{-0.007}$	–
^{61}Co	435.7(5)	431.5(3)	1.4(2)	0.27(4)	1.1(0.3)	$0.39^{+0.16}_{-0.10}$	$7.1^{+2.6}_{-1.6}\times10^{-3}$[e]
^{61}Co	1053.9(7)	1048.7(1.0)	0.7(2)	0.13(4)	$2.4^{+0.6}_{-0.4}$	0.011 ± 0.002	–
^{61}Co	1284.5(6)	1268.7(6)	1.7(2)	0.33(4)	0.8(0.2)	0.019 ± 0.006	–
^{61}Co	1663.8(7)	1662.0(6)	0.2(1)	0.04(2)	10^{+10}_{-3}[f]	$0.37^{+0.31}_{-0.23}$[g]	–
^{63}Co	355.7(4)	353.2(4)	1.0(3)	0.20(6)	$1.7^{+0.8}_{-0.5}$	$0.42^{+0.17}_{-0.14}$	$8.3(2.8)\times10^{-3}$[c]
^{63}Co	407.0(5)	402.6(4)	1.5(3)	0.30(6)	$1.0^{+0.3}_{-0.2}$	0.48 ± 0.11	$9.4^{+1.8}_{-2.2}\times10^{-3}$[c]
^{63}Co	555.9(0.8)	544.0(6)	3.0(2)	0.61(4)	0.3(0.1)	0.63 ± 0.16	$1.2^{+0.6}_{-0.3}\times10^{-2}$[c]
^{63}Co	585.8(1.0)	573.5(1.0)[h]	3.0(6)	0.60(12)	0.3(2)	0.63 ± 0.32	$1.1^{+2.0}_{-0.4}\times10^{-2}$[h]

[a]Lower limit, assumes apparent lifetime values and pure magnetic dipole.
[b]Lower limit.
[c]Partial lifetime for 379 keV magnetic dipole branch $= 49^{+79}_{-23}$ ps.
[d]Obtained using partial lifetime for state from 379 keV decay branch.
[e]See discussion in Sec. IV A.
[f]Partial lifetime for 1664 keV electric quadrupole branch $= 13^{+20}_{-6}$ ps.
[g]Lower limit for $B(E2)$ assuming partial lifetime for 1663 keV $E2$ decay.
[h]Obtained from the proton gated γ-γ data.

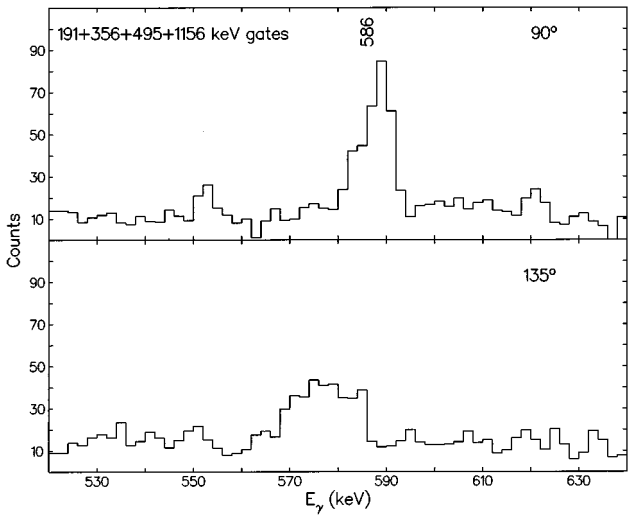

FIG. 11. Sum of the angle projected, proton-γ-γ gates showing the Doppler shifted 586 keV transition in ^{63}Co.

V. COMPARISON WITH SHELL MODEL PREDICTIONS AND PREVIOUS WORK

In order to compare the data with theoretical predictions, the nuclear shell model code OXBASH [26] was used. The model space was truncated to include only protons and neutrons outside an inert ^{48}Ca core. The theoretical energy eigenvalues were then calculated assuming mixtures of pure $(1f_{7/2})^7$ proton states coupled to neutron states arising from the $(1f_{7/2})^{8,8}$, $(2p_{3/2})^{0,4}$, $(1f_{5/2})^{0,6}$, and $(2p_{1/2})^{0,2}$ orbitals using a residual interaction for the fp shell due to van Heese and Glaudemans [27]. The superscripts refer to the minimum and maximum number of particles allowed, respectively, in these shells. The seven valence protons were confined to the $f_{7/2}$ shell and eight neutrons were kept in the corresponding neutron shell at all times. The OXBASH calculation for ^{63}Co was essentially the same as for ^{61}Co but with the extra restriction that there had to be at least two neutrons in the $(1f_{5/2})$ shell. Figures 12 and 13 show the negative parity states with spins greater than $\frac{7}{2}^-$ calculated for both ^{61}Co and ^{63}Co. The calculations predicted many more levels than were observed experimentally below approximately 5 MeV and only the first four predicted states of a given spin (corresponding to the yrast or near-yrast states) are shown.

For ^{61}Co, the qualitative comparison between the experimental and theoretical states is reasonable. The comparison is made assuming negative parity for all of the states observed experimentally, which we repeat does not follow rigorously from the data. It is clear that, experimentally, only the near-yrast states are observed in the current work, consistent with the usual observations for fusion-evaporation reactions. The second lowest $\frac{9}{2}^-$ state predicted in ^{61}Co lies almost 1.5 MeV above the first predicted one and such a state would therefore be heavily unfavored in this type of reaction. (It is worthy of note that a second, highly non-yrast $\frac{9}{2}^-$ state is observed in ^{59}Co [8].) The first three predicted $\frac{11}{2}^-$ states lie below 2.4 MeV in excitation energy with the fourth state another 600 keV higher. Experimentally, only the first two $I=\frac{11}{2}$ states are observed. The yrare $I=\frac{13}{2}$ and

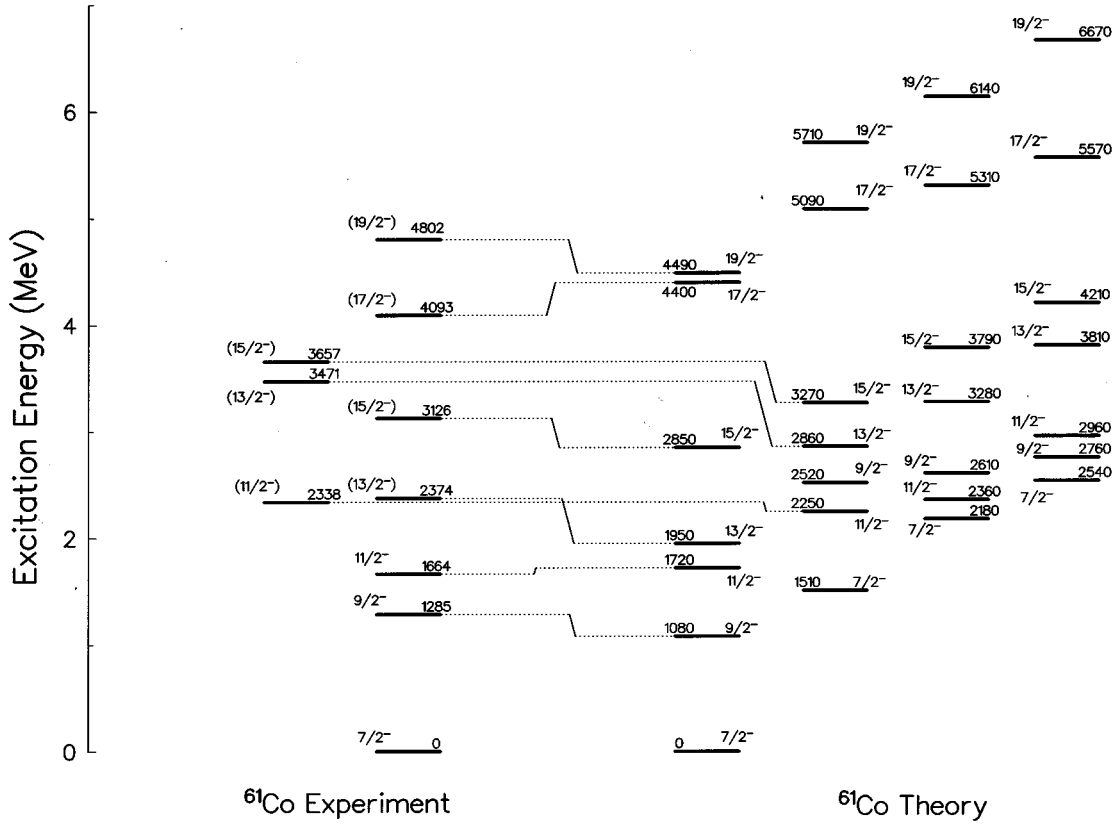

FIG. 12. The lowest lying negative parity levels above spin $\frac{7}{2}^-$ predicted by the shell model for ^{61}Co.

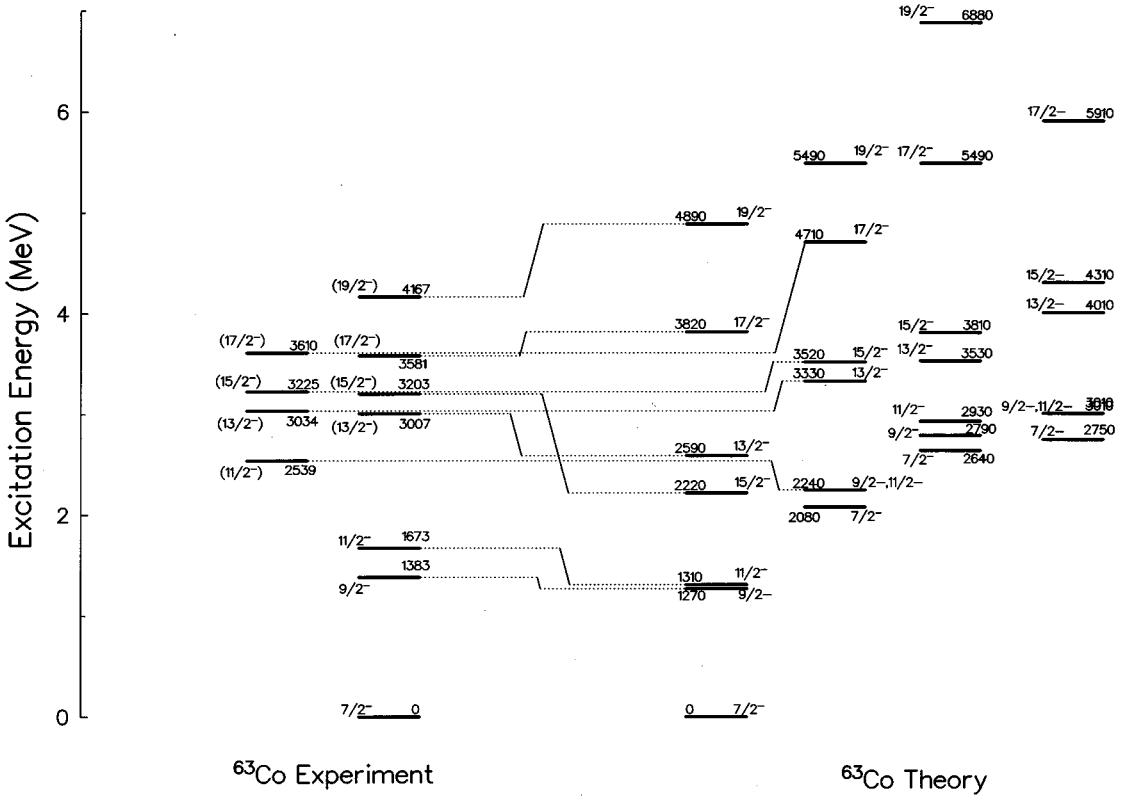

FIG. 13. The lowest lying negative parity levels above spin $\frac{7}{2}^-$ predicted by the shell model for ^{63}Co.

$I=\frac{15}{2}$ states both lie considerably higher in excitation than predicted by the shell model.

For ^{63}Co, as in ^{61}Co, the second predicted $\frac{9}{2}^-$ states lies over 1 MeV higher than the yrast state and indeed experimentally only one $\frac{9}{2}^-$ state is observed. One interesting facet of the calculations for ^{63}Co is that they predict the yrast $\frac{15}{2}^-$ state to lie below the yrast $\frac{13}{2}^-$ state. This is not observed experimentally, with two $I=\frac{13}{2}$ states lying close together at 3007 and 3034 keV, and two $I=\frac{15}{2}$ states lying just above these at 3203 and 3225 keV, respectively.

On a speculative level, it may be possible to associate the unobserved but predicted $\frac{15}{2}^-$ state with the relatively strong, but unplaced, 1248 keV gamma ray. The angular distribution of this transition yields an a_2 value of $+0.38\pm0.29$, consistent with a pure electric quadrupole transition. The large relative intensity of this line would be consistent with a decay from an yrast state. We very tentatively suggest that the 1248 keV transition could originate from an yrast $\frac{15}{2}^-$ state at 2921 keV. However, its placement in the decay scheme cannot be established from the present work. Further study would obviously be required to give a definitive answer on this point.

The relatively high density of states of similar spins makes a precise comparison of the predictions of the shell model for electromagnetic transitions with the data somewhat problematic. Nevertheless, one interesting feature of the data can be so compared. Specifically, in both ^{61}Co and ^{63}Co we note experimentally that the decays of the two lowest probable $\frac{11}{2}^-$ states are qualitatively different. From the measured branching ratios, it follows that the ratio of the $B(E2)$ connecting each $\frac{11}{2}^-$ state to the ground state to the $B(M1)$ connecting the same state to the first $\frac{9}{2}^-$ state is larger by approximately an order of magnitude for the lowest $\frac{11}{2}^-$ state than for the next lowest one. This is consistent with the shell model prediction that the lowest $\frac{11}{2}^-$ state has a much larger $E2$ matrix element to the ground state than the second such state. Thus, the ratio $B(E2)[\frac{11}{2}^-\rightarrow\frac{7}{2}^-]/B(M1)[\frac{11}{2}^-\rightarrow\frac{9}{2}^-]$ is predicted to be 19.2 times larger for the first $\frac{11}{2}^-$ state than for the second in ^{61}Co; the corresponding ratio for ^{63}Co is 23.2. Both are in good agreement with the experimental data noted above, as well as with the expectation that quadrupole strength is concentrated in the lowest available state of a given spin.

The careful study of the yrast states of ^{59}Co by Warburton *et al.* [8] using similar techniques can be compared with the results in the heavier odd-N cobalt isotopes from the present work. Figure 14 shows the experimentally observed excitation energies for the near yrast states in ^{59}Co as observed in Ref. [8] and compares these with the decay schemes obtained for ^{61,63}Co in the present work. The low lying portions of all three decay schemes are rather similar with the observation of yrast $\frac{9}{2}-$ and $\frac{11}{2}^-$ states separated by between 270 and 380 keV. A second, low lying $\frac{11}{2}^{(-)}$ state is also a common feature, although the energy of this state appears to rise with increasing neutron number.

The decay schemes of ^{59}Co and ^{61}Co are very similar for all the observed states in ^{61}Co up to spin $\frac{19}{2}$. With the exception of the very non-yrast states at 3081 ($\frac{9}{2}$), 3843 ($\frac{11}{2}$), and 4177 ($\frac{13}{2}$) keV, respectively, comparable states

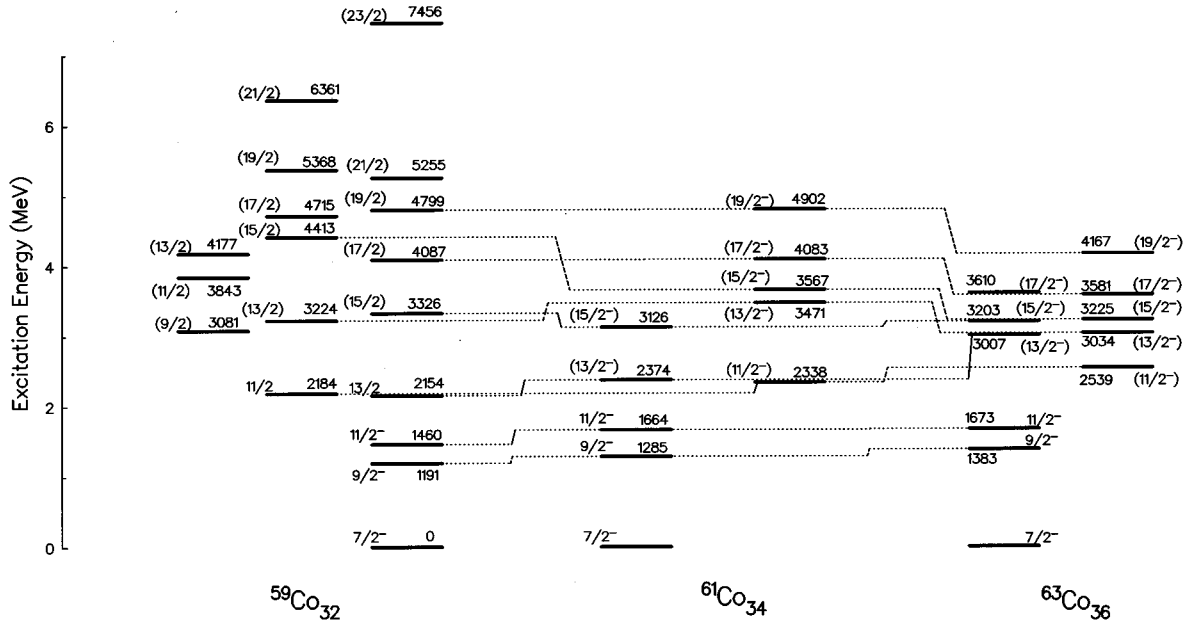

FIG. 14. Comparison of the experimentally observed near-yrast states in the heavy odd-N cobalt isotopes. The data for ^{59}Co come from Ref. [8].

can for the most part be observed in both decay schemes within 250 keV in excitation energy. An exception occurs forthe second $\frac{15}{2}$ state which lies almost 850 keV lower in ^{61}Co compared to ^{59}Co. The energy of this state continues to drop with increasing neutron number and lies a further 342 keV lower in ^{63}Co compared to the analagous state in ^{61}Co.

The energy of both the yrast $I=\frac{17}{2}$ and $\frac{19}{2}$ states drops significantly in ^{63}Co compared to ^{59}Co and ^{61}Co. This may reflect the increasing importance of the high spin $g_{9/2}$ neutron orbital $N=36$ case. There is also a rather dramatic drop in the experimental energies of the yrast $I=\frac{19}{2}$ state and the yrare $I=\frac{17}{2}$ state compared to the energies predicted by the shell model, assuming that the states observed experimentally have negative parity. This may indicate significant occupation of the high spin $g_{9/2}$ neutron orbitals, which are not included in the shell model space, by pairs of particles.

It is worthy of note that the highest spin observed experimentally ($\frac{19}{2}$) is also the highest obtainable for both ^{61,63}Co using the given shell model space (assuming a closed $^{55}_{27}\mathrm{Co}_{28}$ core). The maximal spin configuration is

$$\pi(1f_{7/2})^{-1}{}_{7/2^-}\otimes\nu\{(2p_{3/2})^3{}_{3/2^-}\otimes(1f_{5/2})^3{}_{9/2^-}(\otimes(1p_{1/2})^2{}_0)\}=\tfrac{19}{2}^-. \quad (7)$$

In order to generate states of higher spin, excitations are required either across the $Z=28$ proton shell closure or into the neutron $g_{9/2}$ shell. At low excitation energies (<3.5 MeV), both of these scenarios are energetically unfavored. However, at higher excitation energies states built on such configurations may be expected.

It is probable that the excitation energy of those states involving the neutron $g_{9/2}$ orbital would be lowered with increasing neutron number, as the Fermi surface resides closer to this subshell. As Fig. 14 shows, there is a clear decrease in the energy of the yrast $I=\frac{19}{2}$ state in ^{63}Co compared to both the $A=59$ and 61 isotopes. In ^{59}Co, yrast states of tentative spin $\frac{21}{2}$ and $\frac{23}{2}$ have been observed at 5255 and 7456 keV, respectively, with a second $\frac{21}{2}$ state observed at 6361 keV [8]. No states above spin $\frac{19}{2}$ were observed in the present work.

We have noted that the relatively weak experimental evidence of the present work is consistent with negative parity for all of the levels observed. We note, however, that in the $N=34$ and 36 isotones ^{62,64}Ni there are known non-normal parity states at excitation energies between 3.5 and 4.5 MeV [20,21]. This might suggest the presence of analogous states in ^{61,63}Co with configurations involving an $f_{7/2}$ proton hole coupled to these negative parity states in the corresponding Ni isotopes. The possible existence of such states is noted with interest, and is not completely ruled out for a few states observed in the present study. However, any definitive conclusion on this point must await improved experimental information on the levels involved.

VI. SUMMARY AND CONCLUSIONS

The present work serves as a demonstration that the technique of particle-γ coincidence measurements can be a powerful tool for isolating electromagnetic transitions in relatively neutron rich systems produced in weak fusion-evaporation channels. The extremely clean spectra obtained in measurements of this kind can provide not only coincidence data for level schemes but also detailed line shapes which can give lifetime information. The principal limitation of the present study is the relatively small number of Ge detectors available, which limited the statistical precision with which coincidence relationships could be established. The application of these techniques with the present generation of large detector arrays such as Gammasphere should produce qualitatively better data.

In the present work the decay schemes of the neutron rich isotopes ^{61,63}Co have been investigated using heavy ion fusion reactions and the medium spin yrast states studied for the first time. The number of such states is in reasonable agreement with the predictions of the shell model. Clear evidence of Doppler shifts in some higher lying transitions have been measured, allowing apparent lifetimes to be deduced. A strong decrease is observed in the energy of the yrast $I=\frac{17}{2}$ and $\frac{19}{2}$ states in ^{63}Co compared to ^{59,61}Co, possibly indicating the influence of the neutron $g_{9/2}$ orbitals.

ACKNOWLEDGMENTS

The authors gratefully acknowledge H. White and C. Adams for the operation on the University of Pennsylvania tandem. The assistance of Dr. L. Farriss with performing the experiments is noted with thanks. M.G. McKinzie and Dr. D. F. Winchell are thanked for their help with the shell model calculations. Two of the germanium detectors used in this work were kindly loaned to us by the group at Rutgers University. This work is supported by the National Science Foundation.

[1] R. Araeinejad, J.D. Cole, R.C. Greenwood, S.S. Harrill, N.P. Lohstreter, K. Butler-Moore, S. Zhu, J.H. Hamilton, A.V. Ramayya, X. Zhao, W.C. Ma, J.Kormicki, J.K. Deng, W.B. Gao, I-Y. Lee, N.R. Johnson, F.K. McGowan, G. Ter-Akopian, and Y. Oganessian, Phys. Rev. C **48**, 566 (1993).

[2] J. L. Durell, in *The Spectroscopy of Heavy Nuclei*, 1989, Proceedings of the International Conference on Spectroscopy of Heavy Nuclei, Crete, 1989, edited by J. P. Sharpey-Schafer and L. D. Skouros, IOP Conf. Proc. No. 105 (Institute of Physics, Bristol, 1990), p. 307.

[3] M.A.C. Hotchkis, J.L. Durell, J.B. Fitzgerald, A.S. Mowbray, W.R. Phillips, I. Ahmad, M.P. Carpenter, R.V.F. Janssens, T.L. Khoo, E.F. Moore, L.R. Morss, Ph. Benet, and D. Ye, Phys. Rev. Lett. **64**, 3123 (1990).

[4] M.A.C. Hotchkis, J.L. Durell, J.B. Fitzgerald, A.S. Mowbray, W.R. Phillips, I. Ahmad, M.P. Carpenter, R.V.F. Janssens, T.L. Khoo, E.F. Moore, L.R. Morss, Ph. Benet, and D. Ye, Nucl. Phys. **A530**, 111 (1991).

[5] D.P. Balamuth, U.J. Hüttmeier, and J.W. Arrison, Phys. Rev. C **48**, 2648 (1993).

[6] K. R. Pohl, P. H. Regan, J. E. Bush, P. E. Raines, D. P. Balamuth, D. Ward, A. Galindo-Uribarri, V. P. Janzen, S. M. Mullins, and S. Pilotte, Phys. Rev. C **53**, 2682 (1996).

[7] A.M. Nathan, J.W. Olness, E.K. Warburton, and J.B. McGory, Phys. Rev. C **17**, 1008 (1978).

[8] E.K. Warburton, J.W. Olness, A.M. Nathan, J.J. Kolata, and J.B. McGory, Phys. Rev. C **16**, 1027 (1977).

[9] E.K. Warburton, J.W. Olness, A.M. Nathan, and A.R. Poletti, Phys. Rev. C **18**, 1637 (1978).

[10] J. Bron, H.W. Jongsma, and H. Verhul, Phys. Rev. C **11**, 996 (1975).

[11] E. Runte, K-L. Gippert, W.-D. Schmidt-Ott, P. Tidemand-Petersson, L. Ziegler, R. Kirchner, O. Klepper, P.O. Larsson, E. Roeckl, D. Schart, N. Kaffrell, P. Peuser, M. Bernas, P. Dessagne, M. Langevin, and K. Rykaczewski, Nucl. Phys. **A441**, 237 (1985).

[12] K.L. Coop, I.G. Graham, and E. Titterton, Nucl. Phys. **A150**, 346 (1970).

[13] J.F. Mateja, J.A. Bieszk, J.T. Meek, J.D. Goss, A.A. Rollefson, P.L. Jolivette, and C.P. Brown, Phys. Rev. C **13**, 2269 (1976).

[14] A. G. Blair and D. D. Armstrong, Phys. Rev. C **151**, 930 (1966).

[15] O. Hansen, M.N. Harakeh, J.V. Maher, L.W. Put, and J.C. Vermeulen, Nucl. Phys **A313**, 95 (1979).

[16] M. Seeger, Th. Kihm, K. T. Knopfle, G. Mairle, U. Schmidt-Rohr, J. Hebenstreit, D. Paul, and P. Von Rossen, Nucl. Phys. **A533**, 1 (1991).

[17] T. Chapuran, D.P. Balamuth, J.W. Arrison, and J. Gorres, Nucl. Instrum. Methods A **272**, 767 (1988).

[18] R. Wadsworth, A. Kogan, P.R.G. Lornie, M.R. Nixon, H.G. Price, and P.J. Twin, J. Phys. G **3**, 35 (1977).

[19] F. Pühlhofer, Nucl. Phys. **A280**, 267 (1977).

[20] M.M. King, Nucl. Data Sheets **60**, 337 (1990).

[21] T. Pawlat, R. Broda, W. Krolas, A. Maj, M. Zieblinski, H. Grawe, R. Schubart, K.H. Maier, J. Heese, H. Kluge, and M. Schramm, Nucl. Phys. **A574**, 623 (1994).

[22] P.J. Nolan and J.F. Sharpey-Schafer, Rep. Prog. Phys. **42**, 1 (1979).

[23] T. Alexander and J.S. Forster, *Advances in Nuclear Physics* (Plenum, New York, 1978), Vol. 10, p. 258.

[24] R.D. Lawson, *Theory of the Nuclear Shell Model* (Clarendon Press, Oxford, 1980), p. 274.

[25] P.M. Endt, At. Data Nucl. Data Tables **23**, 547 (1979).

[26] A. Etchegoyen, W.D.M. Rae, N.S. Godwin, W.A. Richter, C.H. Zimmerman, B.A. Brown, W.E. Ormand, and J.S. Winfield (unpublished).

[27] A.G.M. van Heese and P.W.M. Glaudemans, Z. Phys. **303**, 303 (1981).